Journal of Engineering Mathematics 17 (1983) 301–313

A piston-type porous wavemaker theory

A.T. CHWANG and W. LI

Institute of Hydraulic Research, The University of Iowa, Iowa City, Iowa 52242, USA

(Received May 19, 1983)

Summary

The linearized porous wavemaker theory developed by Chwang [3] has been applied to analyze the small-amplitude surface waves produced by a piston-type porous wavemaker near the end of a semi-infinitely long channel of constant depth. Analytical solutions in closed forms are obtained for the free-surface wave profile, the hydrodynamic pressure distribution, and the net force on the wavemaker. The influence of a dimensionless wave-effect parameter C and a dimensionless porous-effect parameter G on the analytical results is discussed. It is found that when the distance between the wavemaker and the channel end-plate is a multiple of the half-wavelength of propagating surface waves, resonance will occur. The "wave-trapping" phenomenon due to resonance is also discussed.

1. Introduction

The classical wavemaker theory developed by Havelock [4], Biesel and Suquet [1], and Ursell et al. [7] has been widely used by investigators to analyze the surface waves produced by wavemakers in open channels, towing tanks, and model basins. In an open channel, a wavemaker is usually installed near the end of the channel and there is a small gap between the wavemaker plate and the side walls of the channel. The influence of leakage flow around the wavemaker on the wave amplitude was analyzed by Madsen [5]. He found that the leakage effect was large in reducing the wave amplitude.

Recently, Chwang [3] developed a porous wavemaker theory to investigate the porous effect of a wavemaker on free-surface gravity waves. In his linearized analysis, a porous wavemaker is located in the middle of an infinitely long channel. He found that the porous effect reduces not only the wave amplitude but also the hydrodynamic pressure force acting on the wavemaker. Therefore, a porous wavemaker may be desirable in situations where efficiency of generation of waves is of main interest with the wavemaker being subjected to some form of structural constraint on the maximum allowable force.

The objective of the present paper is to apply Chwang's theory [3] to analyze small-amplitude surface waves produced by a piston-type porous wavemaker near the end of a semi-infinitely long channel of constant depth. The governing equations and boundary conditions for the present problem are presented in Section 2. Analytical solutions for the hydrodynamic pressure distribution and the total force on the porous wavemaker as well as on the end plate of the channel are presented in Section 3. Results on surface wave profile are discussed in Section 4. In particular, the resonance phenomenon and the associated "wave-trapping" phenomenon are also discussed in that section.

2. Governing equations and boundary conditions

A piston-type porous wavemaker is placed near the end of a semi-infinitely long channel of constant depth (see Fig. 1). The mean position of this porous wavemaker is at $x = 0$ plane and the end plate of the channel is fixed at $x = -L$. The y axis points vertically upwards with the plane $y = 0$ being the bottom of the channel. The porous wavemaker separates the fluid in the channel into two regions; an unbounded region which extends from the wavemaker to infinity along the positive x direction and a finite region between the wavemaker and the end plate. The undisturbed fluid depth in both regions is h. As the wavemaker oscillates along the x-axis with a circular frequency ω and a small horizontal displacement s_0,

$$s_0 = d\,e^{i\omega t} \quad (d \ll h), \tag{1}$$

small-amplitude surface waves are produced in both fluid regions with the disturbed free surface being at $y = h + \eta(x, t)$. We shall assume that the maximum displacement d and the wave amplitude η are very small in comparison with the undisturbed fluid depth h. The corresponding horizontal velocity and acceleration of the wavemaker are

$$u_0 = i\omega d\,e^{i\omega t} \qquad \text{and} \qquad a_0 = -\omega^2 d\,e^{i\omega t}, \tag{2}$$

respectively.

We shall assume the fluid in the channel to be inviscid and incompressible, and its motion irrotational. Therefore, the velocity potentials satisfy the two-dimensional Laplace equation

$$\nabla^2 \Phi_i = 0 \quad (i = 1, 2), \tag{3}$$

where the subscript 1 refers to the unbounded region and 2 refers to the bounded region between the wavemaker and the end plate. The linearized free-surface conditions for the velocity potentials Φ_i are

$$\frac{\partial^2 \Phi_i}{\partial t^2} + g\frac{\partial \Phi_i}{\partial y} = 0 \qquad \text{at} \qquad y = h \quad (i = 1, 2), \tag{4}$$

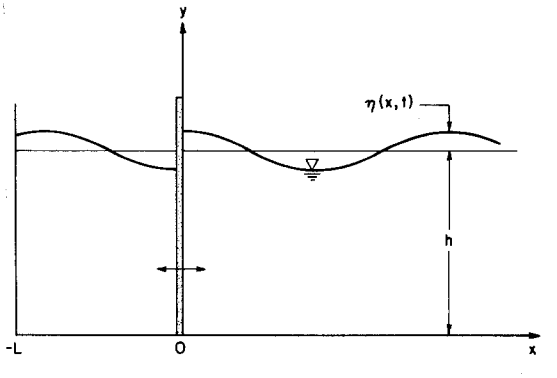

Figure 1. Schematic diagram of a porous wavemaker near the end of a semi-infinitely long channel.

where g is the constant acceleration of gravity. The normal velocity of the fluid must vanish at the bottom of the channel. Therefore

$$\frac{\partial \Phi_i}{\partial y} = 0 \qquad \text{at} \qquad y = 0 \quad (i = 1, 2). \tag{5}$$

On the end plate, the normal velocity also vanishes. Hence

$$\frac{\partial \Phi_2}{\partial x} = 0 \qquad \text{at} \qquad x = -L. \tag{6}$$

If the wavemaker was impermeable, we would require the normal velocities of the fluid on the wavemaker surfaces in both regions be the same as that of the wavemaker. However, the wavemaker is porous. There is a flow between the two fluid regions passing through the pores of the wavemaker. Thus, the fluid in one region is connected by this flow to the fluid in the other region. We cannot solve for Φ_1 or Φ_2 separately. The solutions for Φ_1 and Φ_2 depend on each other through boundary conditions applied on the porous wavemaker.

Let the normal velocity of the fluid passing through the porous wavemaker from the unbounded region to the bounded region be $W(y, t)$. The linearized boundary conditions on both sides of the wavemaker are

$$\frac{\partial \Phi_i}{\partial x} = u_0 - W \qquad \text{at} \qquad x = 0 \quad (i = 1, 2), \tag{7}$$

where u_0 is given by Eqn. (2). We shall assume that the porous wavemaker is made of material with very fine pores and the porous flow through the wavemaker is not significant. Hence, the porous flow velocity W is linearly proportional to the pressure difference between the two sides of the wavemaker [6,3],

$$W(y, t) = \frac{b}{\mu}\left[P_1(0, y, t) - P_2(0, y, t)\right], \tag{8}$$

where μ is the constant coefficient of dynamic viscosity and b is a material constant having the dimension of a length. The hydrodynamic pressures $P_i(x, y, t)$ $(i = 1, 2)$ are related to the velocity potentials through the linearized Bernoulli equation as

$$P_i = -\rho \frac{\partial \Phi_i}{\partial t} \quad (i = 1, 2), \tag{9}$$

where ρ is the constant density of the fluid. We shall note that the hydrodynamic pressure given by (9) is the pressure in excess of the hydrostatic pressure.

3. The hydrodynamic pressure force

Following the approach of Chwang [3], we assume that the velocity potentials Φ_i, the hydrodynamic pressures P_i, and the porous flow W are all periodic functions in t and have

a time factor $\exp(i\omega t)$,

$$\Phi_i = \phi_i(x, y)\, e^{i\omega t}, \qquad P_i = p_i(x, y)\, e^{i\omega t} \quad (i = 1, 2), \tag{10a}$$

$$W = w(y)\, e^{i\omega t}. \tag{10b}$$

The general solution of Eqn. (3) for the unbounded region, satisfying the boundary conditions (4) and (5), was given by Chwang [3] as

$$\phi_1 = A_0 \cosh k_0 y\, e^{-ik_0 x} + \sum_{n=1}^{\infty} A_n \cos k_n y\, e^{-k_n x}, \tag{11}$$

where k_0 satisfies the dispersion relation

$$\omega^2 = g k_0 \tanh(k_0 h) \tag{12}$$

or

$$1 - C k_0 h \tanh(k_0 h) = 0, \tag{13a}$$

the k_n's are the roots of

$$1 + C k_n h \tan(k_n h) = 0 \quad (n = 1, 2, 3, \ldots), \tag{13b}$$

C is a dimensionless wave-effect parameter [2] defined by

$$C = g/(\omega^2 h), \tag{13c}$$

and A_0 and A_n $(n = 1, 2, 3, \ldots)$ are constant coefficients to be determined later by applying the boundary condition on the wavemaker surface. The choice of $\exp(-ik_0 x)$ in Eqn. (11) ensures that the surface waves produced by the porous wavemaker propagate away from the wavemaker. Similarly, the general solution of Eqn. (3) for the bounded region, satisfying the boundary conditions (4), (5), and (6), is obtained by the method of separation of variables as

$$\phi_2 = B_0 \cosh k_0 y \cos k_0 (x + L) + \sum_{n=1}^{\infty} B_n \cos k_n y \cosh k_n (x + L), \tag{14}$$

where B_0 and B_n $(n = 1, 2, 3, \ldots)$ are undetermined Fourier coefficients.

Substituting (11) and (14) into (8), (9), and (10), we have

$$\mu w(y) = -i\omega b \rho \left[(A_0 - B_0 \cos k_0 L) \cosh k_0 y + \sum_{n=1}^{\infty} (A_n - B_n \cosh k_n L) \cos k_n y \right]. \tag{15}$$

Substituting (11), (14), and (15) into (7) and noting that the eigenfunctions $\cosh k_0 y$ and $\cos k_n y$ $(n = 1, 2, 3, \ldots)$ are orthogonal over the interval from $y = 0$ to $y = h$, we obtain

the constant Fourier coefficients as

$$A_0 = -iB_0 \sin k_0 L$$

$$= -\frac{2\omega d Q_0 T_0}{k_0^2 h\left(1 + CQ_0^2\right)}\left[\frac{T_0(1+G_0)+iG_0}{G_0^2 + T_0^2(1+G_0)^2}\right], \tag{16a}$$

$$A_n = -B_n \sinh k_n L$$

$$= -\frac{2\omega d Q_n T_n}{k_n^2 h\left(1 - CQ_n^2\right)}\left[\frac{G_n(1+T_n)+iT_n}{T_n^2 + G_n^2(1+T_n)^2}\right] \quad (n = 1, 2, 3, \ldots), \tag{16b}$$

where

$$Q_0 = \sinh k_0 h, \qquad Q_n = \sin k_n h \quad (n = 1, 2, 3, \ldots), \tag{16c}$$

$$T_0 = \tan k_0 L, \qquad T_n = \tanh k_n L \quad (n = 1, 2, 3, \ldots), \tag{16d}$$

$$G_0 = Gk_1/k_0, \qquad G_n = Gk_1/k_n \quad (n = 1, 2, 3, \ldots), \tag{16e}$$

and

$$G = (\rho\omega b)/(\mu k_1). \tag{16f}$$

We note that the dimensionless porous-effect parameter G defined by (16f) is half of that defined by Chwang [3]. $G = 0$ means that the wavemaker is impermeable. On the other hand, as G approaches to infinity, the porous wavemaker becomes completely permeable or "transparent" to the fluid; in other words, there would be no wavemaker at all in the limit of infinitely large G.

The net hydrodynamic pressure on the porous wavemaker, normalized with respect to $\rho h(-\omega^2 d)$, is (taking the real part only)

$$\frac{P_2(0, y, t) - P_1(0, y, t)}{-\rho\omega^2 dh} = C_{p1}\cos\omega t + C_{q1}\sin\omega t, \tag{17a}$$

where the in-phase (with respect to the horizontal displacement of the wavemaker) pressure coefficient C_{p1} is obtained from Eqns. (9), (10), (11), (14), and (16) as

$$C_{p1} = \frac{2Q_0 T_0 \cosh k_0 y}{k_0^2 h^2\left(1 + CQ_0^2\right)\left[G_0^2 + T_0^2(1+G_0)^2\right]}$$

$$- \sum_{n=1}^{\infty} \frac{2Q_n T_n(1+T_n)\cos k_n y}{k_n^2 h^2\left(1 - CQ_n^2\right)\left[T_n^2 + G_n^2(1+T_n)^2\right]}, \tag{17b}$$

and the out-of-phase pressure coefficient C_{q1} is given by

$$C_{q1} = -\frac{2Q_0\left[G_0 + T_0^2(1+G_0)\right]\cosh k_0 y}{k_0^2h^2\left(1+CQ_0^2\right)\left[G_0^2 + T_o^2(1+G_0)^2\right]}$$

$$-\sum_{n=1}^{\infty}\frac{2Q_nG_n(1+T_n)^2\cos k_n y}{k_n^2h^2\left(1-CQ_n^2\right)\left[T_n^2 + G_n^2(1+T_n)^2\right]}. \tag{17c}$$

Similarly, the hydrodynamic pressure on the end plate of the channel is

$$\frac{P_2(-L, y, t)}{-\rho\omega^2 dh} = C_{p2}\cos\omega t + C_{q2}\sin\omega t, \tag{18a}$$

where the dimensionless pressure coefficients C_{p2} and C_{q2} are

$$C_{p2} = \frac{2Q_0T_0(1+G_0)\cosh k_0 y}{k_0^2h^2\left(1+CQ_0^2\right)\left[G_0^2 + T_0^2(1+G_0)^2\right]\cos k_0 L}$$

$$-\sum_{n=1}^{\infty}\frac{2Q_nT_n\cos k_n y}{k_n^2h^2\left(1-CQ_n^2\right)\left[T_n^2 + G_n^2(1+T_n)^2\right]\cosh k_n L} \tag{18b}$$

and

$$C_{q2} = -\frac{2Q_0G_0\cosh k_0 y}{k_0^2h^2\left(1+CQ_0^2\right)\left[G_0^2 + T_0^2(1+G_0)^2\right]\cos k_0 L}$$

$$-\sum_{n=1}^{\infty}\frac{2Q_nG_n(1+T_n)\cos k_n y}{k_n^2h^2\left(1-CQ_n^2\right)\left[T_n^2 + G_n^2(1+T_n)^2\right]\cosh k_n L} \tag{18c}$$

respectively. The dimensionless pressure distribution may also be expressed as

$$C_{pi}\cos\omega t + C_{qi}\sin\omega t = D_{pi}\cos\left(\omega t - \theta_{pi}\right), \tag{19a}$$

where

$$D_{pi} = \left(C_{pi}^2 + C_{qi}^2\right)^{1/2} \quad (i = 1, 2), \tag{19b}$$

$$\theta_{pi} = \tan^{-1}\left(C_{qi}/C_{pi}\right) \quad (i = 1, 2). \tag{19c}$$

In Fig. 2 the dimensionless pressure distributions D_{p1} and D_{p2} are plotted versus the vertical depth y/h for several different values of G at $C = 0$ and $L/h = 1$. We note from Fig. 2 that for any fixed values of G, both D_{p1} and D_{p2} increase from zero at the free surface, $y = h$, to maximum values at the channel bottom, $y = 0$. At a given depth, D_{p1} and D_{p2} decreases as G increases. This is due to the fact that the wavemaker becomes more

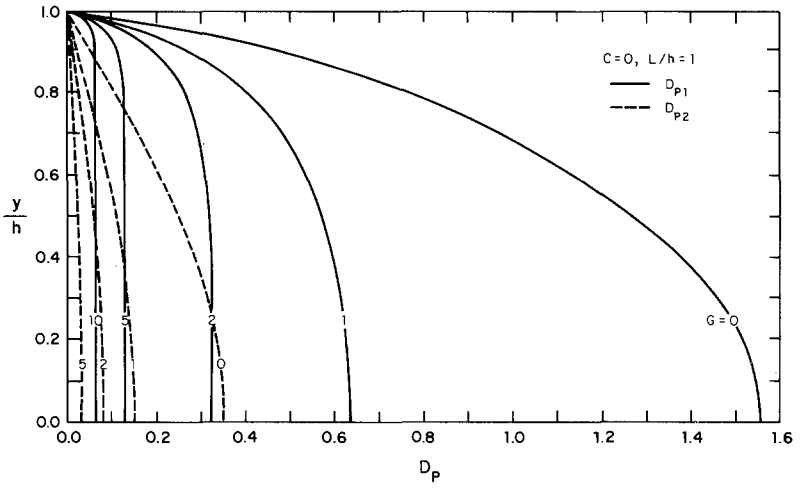

Figure 2. Hydrodynamic pressure distributions on the wavemaker, D_{p1}, and on the end plate, D_{p2}, at $C = 0$ and $L/h = 1$.

porous and thus exerts less force onto the fluid as G increases. With the parameter G and the vertical depth y being fixed, the pressure distribution on the wavemaker, D_{p1}, is always greater than that on the end plate, D_{p2}.

Figure 3 shows the pressure distributions at $C = 0.2$ and $L/h = 1$. As explained by Chwang [2], the wave-effect parameter C is a direct measure of the gravity effect to the inertial effect due to the oscillation of the wavemaker (see Eqn. (13c)). The gravity wave on the free surface becomes dominant for large values of C. We note from Fig. 3 that the pressure distributions, D_{p1} and D_{p2}, are no longer monotonic as in Fig. 2; they oscillate near the free surface. We also note that D_{p1} and D_{p2} do not vanish at the free surface, $y = h$, because of the presence of surface gravity waves. They take values corresponding to the local hydrostatic pressures.

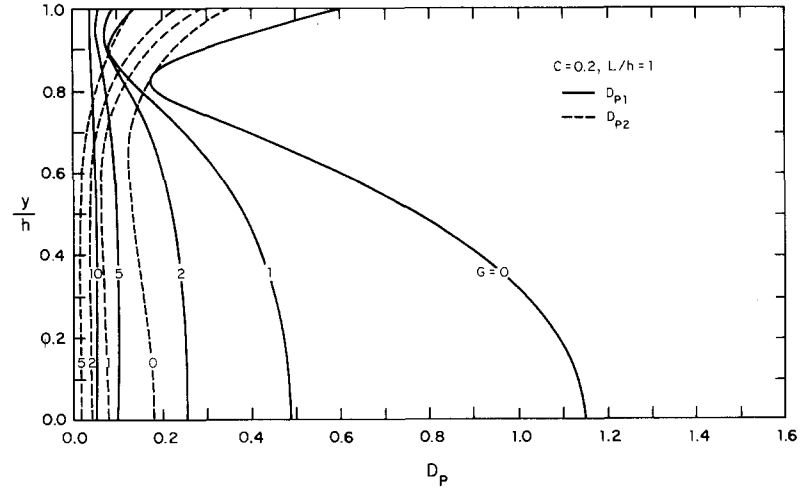

Figure 3. Hydrodynamic pressure distributions on the wavemaker, D_{p1}, and on the end plate, D_{p2}, at $C = 0.2$ and $L/h = 1$.

The total pressure forces on the porous wavemaker and on the end plate, normalized with respect to $\rho h^2\ (-\omega^2 d)$, are obtained by integrating (17) and (18) with respect to y from $y=0$ to $y=h$,

$$C_{Fi}\cos\omega t + C_{Li}\sin\omega t = D_{Fi}\cos(\omega t - \theta_{Fi}), \tag{20a}$$

where

$$D_{Fi} = \left(C_{Fi}^2 + C_{Li}^2\right)^{1/2} \quad (i=1,2), \tag{20b}$$

$$\theta_{Fi} = \tan^{-1}(C_{Li}/C_{Fi}) \quad (i=1,2), \tag{20c}$$

$$C_{F1} = \frac{2Q_0^2 T_0}{k_0^3 h^3\left(1+CQ_0^2\right)\left[G_0^2 + T_0(1+G_0)^2\right]} - \sum_{n=1}^{\infty} \frac{2Q_n^2 T_n(1+T_n)}{k_n^3 h^3\left(1-CQ_n^2\right)\left[T_n^2 + G_n^2(1+T_n)^2\right]}, \tag{20d}$$

$$C_{L1} = -\frac{2Q_0^2\left[G_0 + T_0^2(1+G_0)\right]}{k_0^3 h^3\left(1+CQ_0^2\right)\left[G_0^2 + T_0^2(1+G_0)^2\right]} - \sum_{n=1}^{\infty} \frac{2Q_n^2 G_n(1+T_n)^2}{k_n^3 h^3\left(1-CQ_n^2\right)\left[T_n^2 + G_n^2(1+T_n)^2\right]}, \tag{20e}$$

$$C_{F2} = \frac{2Q_0^2 T_0(1+G_0)}{k_0^3 h^3\left(1+CQ_0^2\right)\left[G_0^2 + T_0^2(1+G_0)^2\right]\cos k_0 L} - \sum_{n=1}^{\infty} \frac{2Q_n^2 T_n}{k_n^3 h^3\left(1-CQ_n^2\right)\left[T_n^2 + G_n^2(1+T_n)^2\right]\cosh k_n L}, \tag{20f}$$

$$C_{L2} = -\frac{2Q_0^2 G_0}{k_0^3 h^3\left(1+CQ_0^2\right)\left[G_0^2 + T_0^2(1+G_0)^2\right]\cos k_0 L} - \sum_{n=1}^{\infty} \frac{2Q_n^2 G_n(1+T_n)}{k_n^3 h^3\left(1-CQ_n^2\right)\left[T_n^2 + G_n^2(1+T_n)^2\right]\cosh k_n L}. \tag{20g}$$

The dimensionless force on the wavemaker, D_{F1}, is plotted in Fig. 4 versus $1/C$ for three different values of G at $L/h=1$. For an impermeable wavemaker, $G=0$, we note from Eqns. (20) and (16) that C_{F1}, and hence D_{F1}, goes to infinity as T_0 tends to zero. By (16d), T_0 vanishes when $k_0 L = m\pi$ $(m=0, 1, 2, \ldots)$. Since the wavenumber k_0 is equal to $2\pi/\lambda$, where λ is the wavelength of the surface waves produced by the wavemaker,

$$T_0 = 0 \qquad \text{when} \quad L = m(\lambda/2) \quad (m=1, 2, 3, \ldots). \tag{21}$$

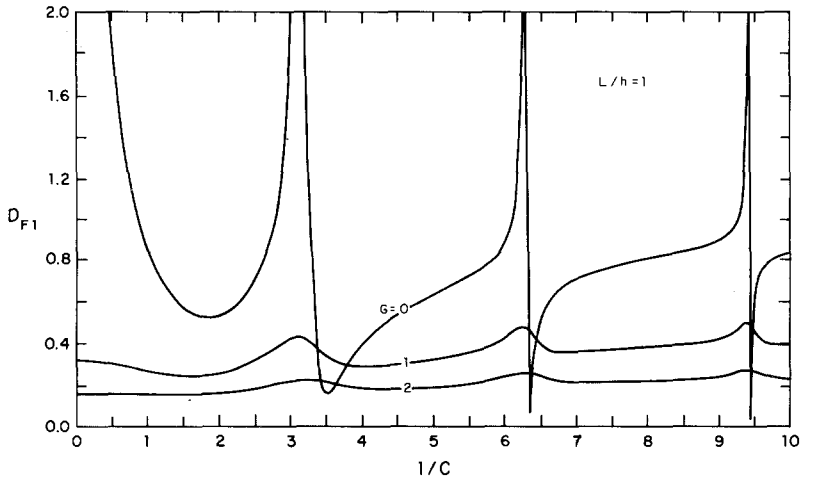

Figure 4. The dimensionless net force on the wavemaker for $L/h = 1$.

In Eqn. (21), $m = 0$ is excluded because L is always positive. Therefore, when the length of the finite fluid region, L, is a multiple of the half-wavelength of propagating surface waves, resonance will occur. Alternatively, for fixed length L/h, D_{F1} goes to infinity as

$$\frac{1}{C} = m\pi(h/L)\tanh(m\pi h/L), \tag{22}$$

where m is any positive integer and Eqn. (13a) is applied in deriving (22). For finite values of C, Fig. 4 shows that resonance occurs when $1/C$ is around π, 2π, 3π, etc. for $G = 0$ and $L/h = 1$. For a porous wavemaker, $G > 0$, D_{F1} is always finite even at resonant values of $1/C$.

For a fixed value of the porous-effect parameter G, $G = 1$, Fig. 5 shows the dimensionless force D_{F1} versus $1/C$ at three different values of L/h. Although D_{F1} is always finite at

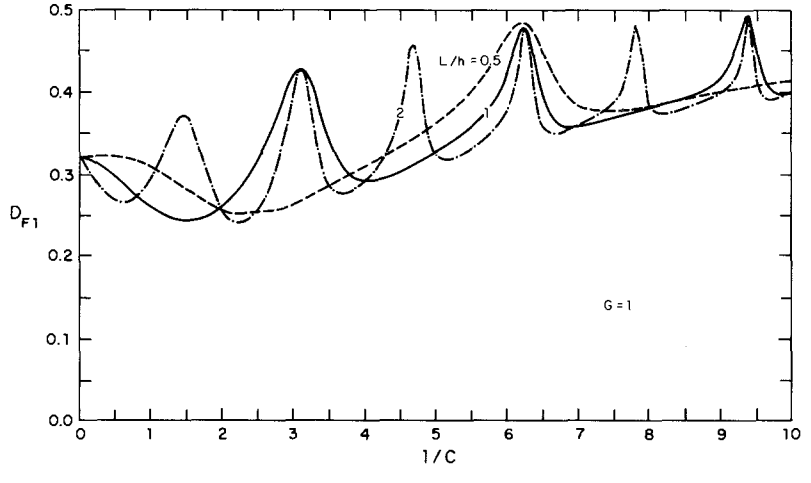

Figure 5. The dimensionless net force on the wavemaker for $G = 1$.

$G = 1$, it reaches local peak values at resonant values of $1/C$ corresponding to an impermeable wavemaker.

4. Surface wave profile

The free surface elevation measured from the undisturbed fluid level at $y = h$, $\eta(x, t)$, is related to the velocity potentials by the linearized dynamic conditions at the free surface

$$\eta(x, t) = -\frac{1}{g}\frac{\partial \Phi_i}{\partial t} \qquad \text{at} \quad y = h \quad (i = 1, 2). \tag{23}$$

Substituting (10), (11), and (16) into (23) and taking the real part only, we obtain the surface wave profile in the unbounded region

$$\eta_1/d = E_0 \sin(k_0 x - \omega t) - F_0 \cos(k_0 x - \omega t) + \sum_{n=1}^{\infty} (E_n \cos \omega t + F_n \sin \omega t)\, \mathrm{e}^{-k_n x}, \tag{24a}$$

where

$$E_0 = \frac{2Q_0^2 T_0^2 (1 + G_0)}{k_0 h (1 + CQ_0^2)\left[G_0^2 + T_0^2 (1 + G_0)^2\right]}, \tag{24b}$$

$$F_0 = \frac{2Q_0^2 T_0 G_0}{k_0 h (1 + CQ_0^2)\left[G_0^2 + T_0^2 (1 + G_0)^2\right]}, \tag{24c}$$

$$E_n = \frac{2Q_n^2 T_n^2}{k_n h (1 - CQ_n^2)\left[T_n^2 + G_n^2 (1 + T_n)^2\right]}, \tag{24d}$$

$$F_n = \frac{2Q_n^2 T_n G_n (1 + T_n)}{k_n h (1 - CQ_n^2)\left[T_n^2 + G_n^2 (1 + T_n)^2\right]}. \tag{24e}$$

Similarly, the disturbed free surface elevation in the bounded region between the porous wavemaker and the end plate is obtained from (10), (14), (16), and (23) as

$$\eta_2/d = (H_0 \cos \omega t + I_0 \sin \omega t) \cos k_0 (x + L) + \sum_{n=1}^{\infty} (H_n \cos \omega t + I_n \sin \omega t) \cosh k_n (x + L), \tag{25a}$$

where

$$H_0 = -\frac{2Q_0^2 T_0 (1 + G_0)}{k_0 h (1 + CQ_0^2)\left[G_0^2 + T_0^2 (1 + G_0)^2\right] \cos k_0 L}, \tag{25b}$$

$$I_0 = \frac{2Q_0^2 G_0}{k_0 h\left(1 + CQ_0^2\right)\left[G_0^2 + T_0^2(1 + G_0)^2\right] \cos k_0 L}, \tag{25c}$$

$$H_n = -\frac{2Q_n^2 T_n}{k_n h\left(1 - CQ_n^2\right)\left[T_n^2 + G_n^2(1 + T_n)^2\right] \cosh k_n L}, \tag{25d}$$

$$I_n = -\frac{2Q_n^2 G_n(1 + T_n)}{k_n h\left(1 - CQ_n^2\right)\left[T_n^2 + G_n^2(1 + T_n)^2\right] \cosh k_n L}. \tag{25e}$$

We note from (24a) that the free-surface gravity waves propagate in the positive x direction away from the wavemaker in the unbounded fluid region. On the other hand, both incident and reflected waves are present in finite region between the wavemaker and the end plate as seen from Eqn. (25a). Figure 6 shows a typical wave profile in a semi-infinitely long channel for different values of G at $C = 0.2$, $\omega t = 0$, and $L/h = 1$. We note from Fig. 6 that surface waves due to an impermeable wavemaker ($G = 0$) have the largest amplitude, and the amplitude of the wave decreases as the porous-effect parameter G increases. This is quite understandable because the wavemaker becomes more porous as G gets larger. Figure 6 also shows that the wave amplitude decreases away from the wavemaker for any fixed values of G. The influence of the wave-effect parameter C on the surface wave profile is shown in Fig. 7 for an impermeable wavemaker at $\omega t = 0$ and $L/h = 1$. We observe from Fig. 7 that as C increases from 0.2 to 0.4, the wave amplitude decreases while the wavelength almost doubles. At $C = 0$, surface gravity waves cease to exist and the free surface profile resembles that due to a dipole at $x = 0$ plane, which is the mean position of the wavemaker.

The final output curves of a piston-type porous wavemaker are presented in Figs. 8 and 9. In Fig. 8 the wave amplitude at infinity, $(E_0^2 + F_0^2)^{1/2}$, is plotted versus $1/C$ for three different values of G at $L/h = 1$; whereas in Fig. 9 G is fixed at one, but L/h takes the values of 0.5, 1, and 2. We note from Fig. 8 that the wave amplitude decreases as G increases for fixed $1/C$ as explained before. As C approaches to zero or $1/C$ tends to

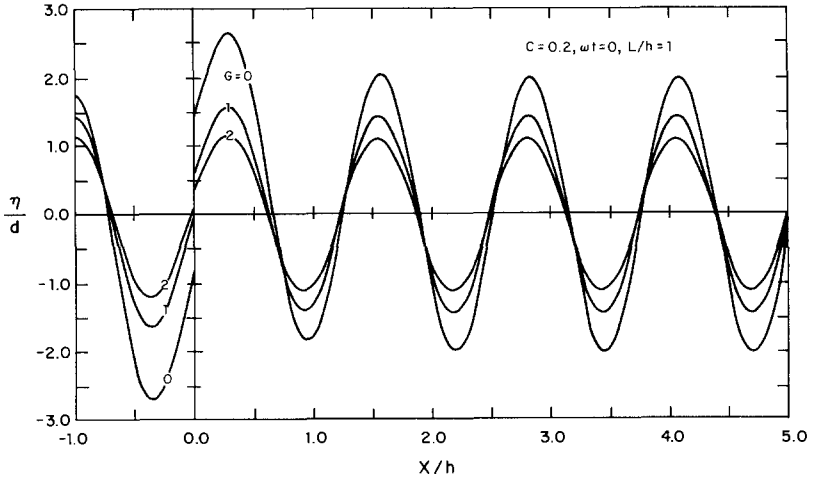

Figure 6. Surface wave profile at $C = 0.2$, $\omega t = 0$, and $L/h = 1$.

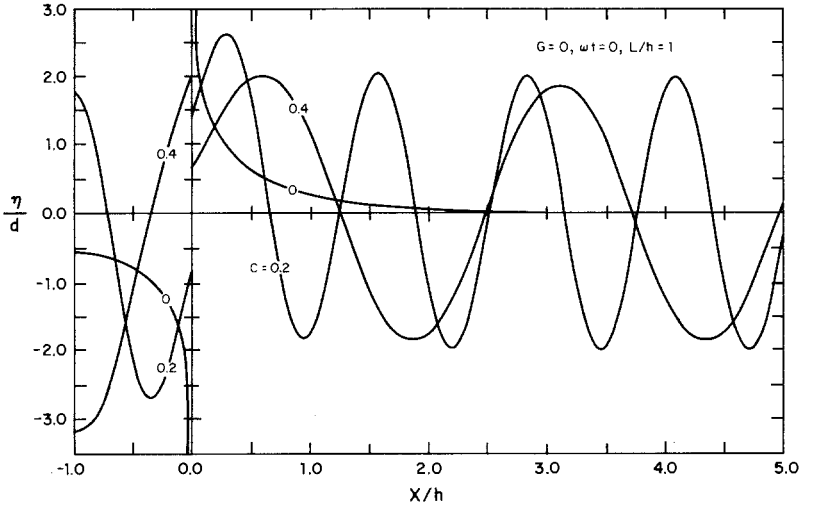

Figure 7. Surface wave profile at $G = 0$, $\omega t = 0$, and $L/h = 1$.

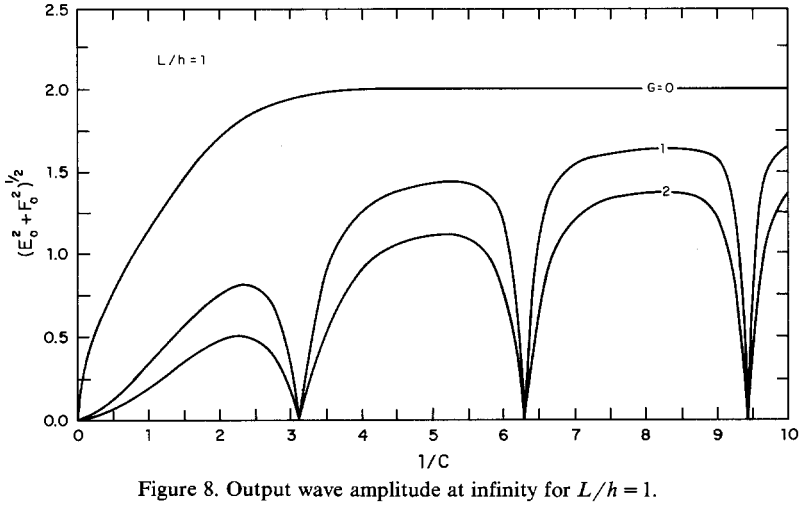

Figure 8. Output wave amplitude at infinity for $L/h = 1$.

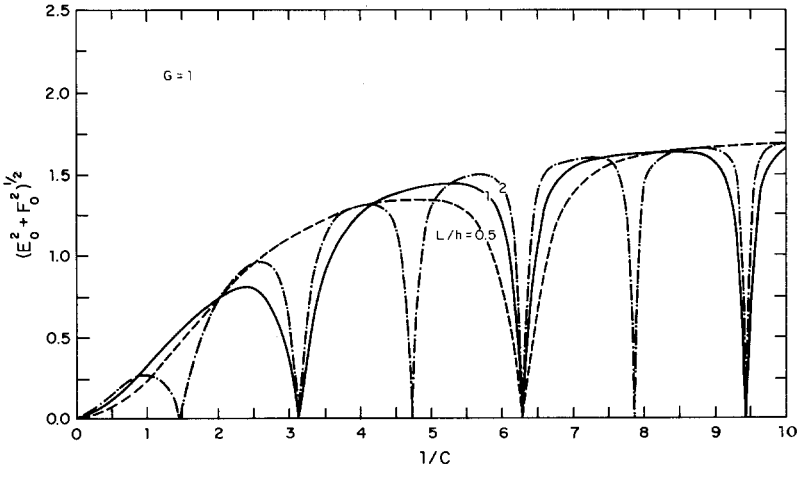

Figure 9. Output wave amplitude at infinity for $G = 1$.

infinity, the wave amplitude approaches to the limiting value of 2 regardless of the values of G. For non-vanishing values of G, there is a "wave-trapping" phenomenon. That is, waves will be trapped inside the channel when L is a multiple of the half-wavelength of surface waves (see Eqns. (21) and (22)); the wave amplitude at infinity tends to zero. The dependence of the ultimate wave amplitude on the distance between the porous wavemaker and the end plate, L/h, is shown in Fig. 9 for $G = 1$. We note from Fig. 9 that the interval of $1/C$ for wave-trapping to occur is doubled when L/h is halved. The ultimate wave amplitude approaches to 2 as $1/C$ tends to infinity for non-resonant values of $1/C$.

Acknowledgement

This work was partially sponsored by the National Science Foundation and by the Office of Naval Research through the Special Focus Research Program in Ship Hydrodynamics under Contract N00014-83-K-0136.

References

[1] F. Biesel and F. Suquet, Les appareils generateurs de houle en laboratoire. *La Houille Blanche* 6 (1951) 147–165, 475–496, 723–737.
[2] A.T. Chwang, Effect of stratification on hydrodynamic pressures on dams. *J. Eng. Math.* 15 (1981) 49–63.
[3] A.T. Chwang, A porous wavemaker theory. *J. Fluid Mech.* 132 (1983) 395–406.
[4] T.H. Havelock, Forced surface-waves on water. *Phil. Mag.* 8 (1929) 569–576.
[5] O.S. Madsen, Waves generated by a piston-type wavemaker. *Proc. 12th Coast. Eng. Conf., ASCE* (1970) 589–607.
[6] G.I. Taylor, Fluid flow in regions bounded by porous surfaces. *Proc.* Roy. Soc. A234 (1956) 456–475.
[7] F. Ursell, R.G. Dean and Y.S. Yu, Forced small-amplitude water waves: a comparison of theory and experiment. *J. Fluid Mech.* 7 (1960) 33–52.